AJNR

An Automated Technique for Measuring Hippocampal Volumes from MR Imaging Studies

Karen M. Gosche, James A. Mortimer, Charles D. Smith, William R. Markesbery and David A. Snowdon

AJNR Am J Neuroradiol 2001, 22 (9) 1686-1689
http://www.ajnr.org/content/22/9/1686

AJNR Am J Neuroradiol 22:1686–1689, October 2001

Technical Note

An Automated Technique for Measuring Hippocampal Volumes from MR Imaging Studies

Karen M. Gosche, James A. Mortimer, Charles D. Smith, William R. Markesbery, and David A. Snowdon

Summary: We describe an automated volumetric measure of the hippocampus obtained with software called the Knowledge-Guided MRI Analysis Program (KGMAP). Postmortem MR images from 56 participants in the Nun Study were used to validate the measure. KGMAP-determined volumes strongly correlated with those obtained with manual tracings and neurofibrillary pathologic findings of Alzheimer disease in the hippocampus. KGMAP provides a rapid and accurate estimate of hippocampal volume that is suitable for use in clinical practice.

The growing interest in early detection of Alzheimer disease (AD) has generated a need for accurate and efficient methods to estimate volumes of brain structures from MR imaging data. Although a definitive determination of the regions affected first in AD remains unresolved (1−5), neuropathologic as well as MR imaging data suggest that the hippocampus is one of the earliest structures involved. Region-of-interest (ROI) tracing techniques, which represent the current state of the art, are time-consuming and susceptible to intra- and interoperator differences (6). In this article, we describe an automated volumetric measure of the hippocampus obtained with software called the Knowledge-Guided MRI Analysis Program (KGMAP).

Methods

Postmortem MR imaging was performed in participants of the Nun Study (7), a longitudinal study of aging and AD. The 678 participants in the study were members of the School Sisters of Notre Dame congregation. Cognitive and physical function was assessed annually, and all participants agreed to brain donation at death. Postmortem MR imaging was initiated in 1996, and the present sample constituted the findings in the first 56 nuns who underwent imaging.

The whole brain was removed from a formalin solution, inspected for cuts or gross lesions, and immersed in cold water for 15 min. It was then placed in a watertight plastic cylinder containing a dilute formalin solution and rotated to remove bubbles and trapped air from the ventricles. Paper packing was used to prevent movement of the brain within the container during imaging. This inner container was anchored in an outer water-filled loader aligned with fiducial markers. The loader was carefully centered in the head coil by using the same fiducial markers.

MR Imaging

MR imaging was performed with a 1.5-T unit. Three types of images were obtained. First, we obtained axial T2-weighted images with the following parameters: 2500/20 and 80 (TR/TE); field of view (FOV), 256 mm; matrix, 256 × 256; flip angle, 90°; number of signals acquired, one; section thickness, 3 mm interleaved; section gap, 3 mm; sections, 18; and resolution, 1 × 1 × 3 mm. This series was repeated after an axial shift of 3 mm to create a total of 36 sections with no gap and minimal intersection radio-frequency interference.

Second, we obtained coronal magnetization-prepared rapid gradient-echo (MP-RAGE) images with the following parameters: 11.4/4.4; FOV, 256 mm; matrix, 256 × 256; flip angle, 8°; number of signals acquired, one ; section thickness, 2 mm; sections, 180; resolution, 1 × 1 × 2 mm. Because the acquisition was truly 3D, no section gaps and no intersection interference were present.

Third, axial T1-weighted images were obtained with the following parameters: 400/12; FOV, 256 mm; matrix, 512 × 512; flip angle, 90° number of signals acquired, one; section thickness, 3 mm interleaved; section gap, 3 mm; sections, 18; resolution 0.5 × 0.5 × 3 mm. The series was repeated after an axial shift of 3 mm to create a total of 36 sections with no gap and minimal intersection radio-frequency interference.

Of the first 56 MR imaging cases in the Nun Study, we selected 12 for correlation of the manual ROI tracing and automated KGMAP volumetric findings. Four cases were randomly selected from each of three categories representing large, medium, and small hippocampal volumes, as determined with KGMAP. Of the 12 total MR imaging cases selected for these analyses, one case was excluded because of missing data. The remaining 11 cases included a wide range of AD neuropathologic conditions and dementia, with six fulfilling AD neuropathologic criteria (three dementia and three nondementia) and five not fulfilling AD neuropathologic criteria (two dementia and three nondementia).

Two highly trained, independent operators performed ROI tracing with the assistance of Analyze 7c Software (Mayo Clinic Ventures, Rochester, MI) by using the T1-weighted 3D MP-RAGE images. The images were interpolated to a 256 × 256 × 256 matrix and reformatted into the oblique coronal plane perpendicular to the long axis of the hippocampal body. Two-millimeter-thick sections were traced from the tip of the temporal lobe to the most posterior section in which the midbrain colliculi were seen. The outline of the temporal lobe was

Received January 3, 2001; accepted after revision May 31, 2001.

From the Institute on Aging (K.M.G., J.A.M.), University of South Florida, Tampa; and the Departments of Neurology (C.D.S.), Pathology and Neurology (W.R.M.), and Preventive Medicine (D.A.S.), College of Medicine, University of Kentucky, Lexington.

This study was funded by grants R01AG09862 and K04AG00553 (D.A.S.) and 5P50AG05144 (W.R.M.) from the National Institute on Aging and by grants from the Kleberg Foundation and the Abercrombie Foundation.

Address reprint requests to Karen M. Gosche, Institute on Aging, University of South Florida, MDC-56, 13201 Bruce B. Downs Boulevard, Tampa, FL 33612-3899.

traced on each section, and the outlines of the amygdala and hippocampus were traced on the sections in which they appeared.

The posterior boundary of the hippocampus and temporal lobe was set at the level of the last section on which the midbrain collicular plate appeared. For the hippocampus, the choroid fissure was the superior boundary, the inferior temporal horn of the lateral ventricle was the lateral boundary, and the white matter of the parahippocampal gyrus was the inferior boundary. Anteriorly, the white matter of the alveus delineated the boundary between the hippocampus and amygdala. If the delineation between the amygdala and hippocampus was not seen, the tracing followed the lateral and inferior boundaries to the medial edge of the gray matter; a straight horizontal line then was drawn to the beginning of the trace at the lateral edge. The resulting outlined areas were used to calculate the estimated left and right hippocampal volumes.

A neuropathologist who was unaware of the participants' neuropathology cognitive test scores performed gross and microscopic evaluations of the brains after MR imaging. For histopathologic evaluation, multiple sections of the neocortex, hippocampus, entorhinal cortex, amygdala, basal ganglia, brain stem, and cerebellum were stained with hematoxylin and eosin and the modified Bielschowsky stain. Sections of the hippocampus and entorhinal cortex also were stained by using the Gallyas method. Senile plaques (both diffuse and neuritic types) and neurofibrillary tangles (NFTs) were counted in Bielschowsky stained sections of the five most severely involved microscopic fields of the middle frontal gyrus (Brodmann area 9), inferior parietal lobule (areas 39 and 40), middle temporal gyrus (area 21), CA-1 region and subiculum of the hippocampus.

In addition, brains were staged for the severity of neurofibrillary disease with the criteria proposed by Braak and Braak (8) by using Gallyas and Bielschowsky stains. Braak and Braak (8) divided the neuropathologic progression of AD into six stages on the basis of the distribution of NFTs and neuropil threads. In stages I and II, neurofibrillary degeneration is restricted to the transentorhinal region. Stages III and IV include wider involvement of the limbic system, whereas stages V and VI are associated with neurofibrillary degeneration in the isocortex.

Computer Algorithm

Volumetric measures were obtained by using KGMAP, an automated computer algorithm. The details of KGMAP have been modified since its original description (9). The program had been written to detect hyperintensities in the brain and thus was called Knowledge-Guided Hyperintensity Detection. As the program logic was expanded, the name was changed to the current Knowledge-Guided MRI Analysis Program, to better reflect its capabilities. Since the first publication, technical changes have consisted primarily of enhancements to prior logic and additions of new logic to detect and analyze additional structures of interest. One such addition is the logic that localizes the hippocampi. The procedure of isolating the hippocampus uses the location of the lateral ventricle and the separation of gray matter and white matter.

To summarize KGMAP, the knowledge rules written into this algorithm are based on intensities combined with the spatial relationship of anatomic structures. These rules, used together, result in the localization and identification of regional structures of interest throughout the brain. Once identified, the volume of each region is calculated, and regional analyses are performed.

KGMAP analyses begin with the identification of the lateral ventricles, caudate nuclei, lenticular nuclei, and thalamus on the first image. In the current version, the operator is required to select the first image. However, future enhancements of the program will eliminate the need for operator selection. The locations of these structures, once identified, are used to identify their possible presence in later sections.

Localization of the lateral ventricles begins on the first image by identifying all possible CSF pixels, as indicated by their hyperintense appearance on the T2-weighted image. This procedure results in an approximate representation of all CSF regions confined within the lateral ventricles and sulci. The CSF in the lateral ventricle is uniquely identified on the image by applying an iterative region-growing operation to an initial horizontal line of 31 pixels, in which the midpoint of the line is positioned at the midpoint of the intracranial tissue. The intracranial midpoint is calculated as the point in the image that corresponds to the intersection of the mean x and y coordinates of the tissue. With each growth iteration, horizontal lines are generated and moved vertically one position at a time to capture possible CSF pixels that correspond with the position of the line. The length of each new line is horizontally adjusted and guided by the most lateral occurrence of lateral-ventricle CSF identified in the previous line. This procedure continues until possible lateral ventricle CSF pixels, corresponding with previous locations, are no longer detected. This region-growing process creates a mask that resembles the shape of the lateral ventricles.

CSF pixels are then grouped into regions by using a region-labeling operation. CSF regions that constitute the lateral ventricles are identified as those regions that have a nonempty intersection with the mask just generated.

Once identified, the lateral ventricle is divided both vertically and horizontally; its anatomic shape guides this process. The vertical division is defined as the midpoint between its maximum and minimum location with respect to the x axis. The horizontal division occurs where its width is minimal. To assist in the localization of the caudate and lenticular nuclei, the upper half of the lateral ventricle is further divided into three distinct regions, defined as superior, central, and inferior to the caudate curvatures. These curvatures, occurring bilaterally with respect to the vertical division, appear as concave regions in the exterior wall of the lateral ventricle.

The superior border of each curvature is defined as the point where the horizontal position of the pixels for the lateral ventricle reach their absolute maximum distances from the vertical dividing line. The inferior border of the caudate curvature is defined in a similar manner. By moving inferiorly to the superior border, the inferior border is defined as the location where pixels for the lateral ventricle reach their absolute maximum distances after reaching their absolute minimum distance. The central region of the caudate curvature then is defined as the area between its superior and inferior borders.

The range and average pixel intensities for the lateral ventricle are used to adjust the initial mask of CSF previously identified. This procedure is used to identify all remaining CSF in the sulci. Once all CSF is identified, the pixel intensities of the remaining tissue are used to segment tissue into white matter and gray matter.

As with all other structures, KGMAP begins searching for the hippocampus on the first image. The hippocampus typically does not begin to appear, however, until the image in which the temporal horn and body of the lateral ventricle separate in the axial plane. This generally occurs within two axial images below the first image that KBMAP analyzes. As the analysis of KGMAP progresses downward from the first image into the temporal lobe of the brain, the gray matter that constitutes the hippocampus first is identified as the tissue in the space separating the temporal horn and body of the lateral ventricle. In the axial plane, its superior border lies inferior to the remaining body of the lateral ventricle, whereas its lateral and inferior borders lie medial and superior to the temporal horn of the lateral ventricle. In the case of minimal atrophy, the CSF in this region can be convoluted by partial volume effects in the surrounding tissue. If a strong indication of CSF is not present, the lateral and inferior borders are identified by

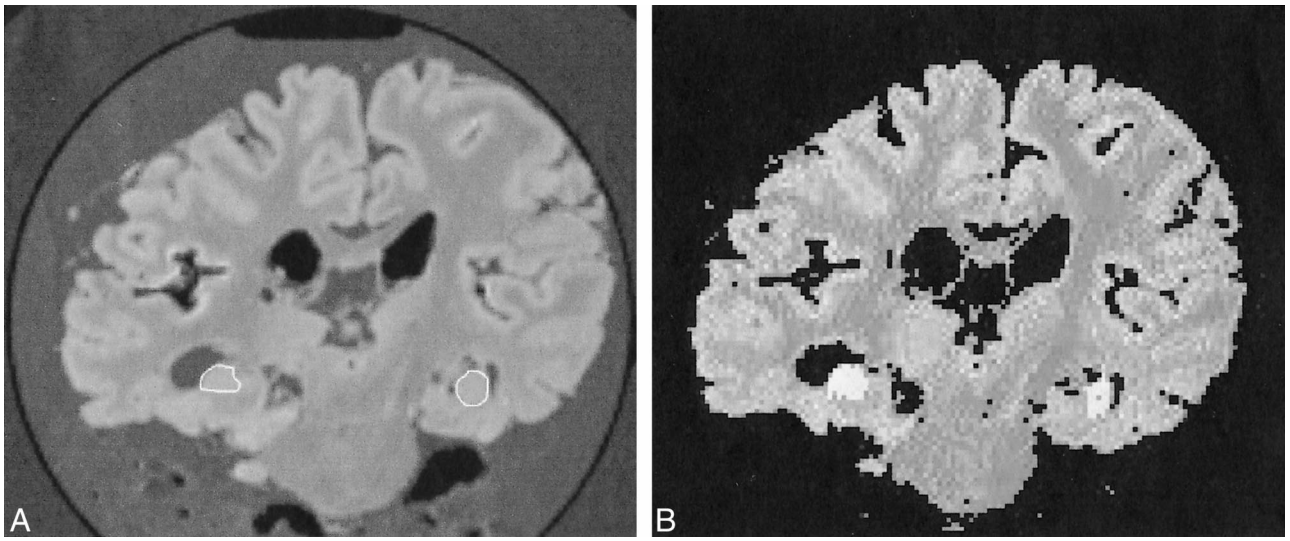

FIG 1. Coronal MP-RAGE (11.4/4.4, 8° flip angle) images from a single participant.
A, Hippocampi manually traced.
B, Pixels identified with the algorithm as belonging to the hippocampi (bright white pixels).

TABLE 1: Correlation between hippocampal volumes estimated by two independent operators and those determined with KGMAP

Hippocampal Volumes	Operator 1 versus Operator 2		Operator 1 versus KGMAP		Operator 2 versus KGMAP	
	r	*P*	*r*	*P*	*r*	*P*
Left	0.85	.003	0.81	.008	0.79	.011
Right	0.64	.060	0.78	.014	0.64	.062

using pixels that indicate the strong presence of white matter. If these procedures do not completely isolate these borders, the algorithm generates an interpretative line, aided with the use of pixels that were found, to close the bordering line.

In a similar manner, the amygdala is differentiated from the body of the hippocampus with an average-to-strong indication of white matter. This demarcation usually is unclear, and again, an interpretive line often is required. The use of hippocampal pixel locations from previous sections greatly aid in the total identification of this structure. Volumetric measures are calculated by using a summation procedure that includes all images that identify the hippocampus.

Figure 1 shows the results of manual tracing of the left and right hippocampi in one individual and, on the same coronal section, the areas identified by the algorithm as the hippocampus.

Validation

Table 1 gives the intraclass correlations between manual tracing results of the two highly trained independent operators. Both operators obtained volumes for the right and left hippocampi in 11 brains. The operators were unaware of each other's results, the volumes calculated by KGMAP, and all neuropathologic and neuropsychologic data. Only left hippocampal volumes were significantly correlated between the operators.

Correlations between manual tracing results of two highly trained independent operators and KGMAP results also are shown in Table 1. The correlations between KGMAP and operator 2 were significant only for left hippocampal volumes, whereas correlations between KGMAP and operator 1 were significant for both left and right hippocampal volumes.

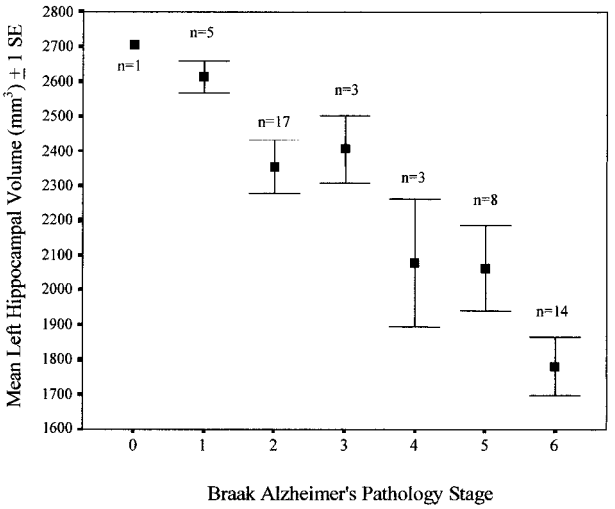

FIG 2. Left hippocampal volume obtained from KGMAP plotted against Braak AD pathologic stage in 51 participants from the Nun Study. Data in five individuals with a dementia other than AD were omitted from the plot.
Values shown are mean ± standard error.

KGMAP-determined hippocampal volumes also were validated by assessing their correlation with measures of hippocampal neuropathologic findings. The Braak stage was determined in all 56 cases in the left side of the brain. When age at death was controlled, a strong correlation between KGMAP hippocampal volume on the left side and the Braak stage existed (partial $r = -0.68$; $P < .001$). Of the 56 cases, five, all with a Braak stage of I or II, were reported to involve dementia due to causes other than AD. Removal of these cases moderately increased the correlation ($r = -0.71$; $P < .001$). Figure 2 shows mean left hippocampal volumes for the 51 remaining cases plotted against the Braak stage.

KGMAP-derived hippocampal volumes strongly correlated with senile plaque and NFT counts in the subiculum and the CA-1 region of the hippocampus (Table 2).

Discussion

KGMAP, an automated computer algorithm, generates estimates for hippocampal volume that were

TABLE 2: Partial correlation of KGMAP-determined left hippocampal volumes with neuropathologic indices in the left hippocampus

Count	*r**	*P*
Mean NFT		
CA-1 region	−0.67	<.001
Subiculum	−0.57	<.001
Mean senile plaque		
CA-1 region	−0.42	<.01
Subiculum	−0.36	<.05

* Adjusted for age at death.

strongly correlated with estimates derived from independently blinded assessments determined by using manual ROI tracing. Furthermore, the volumes obtained with this algorithm were highly correlated with the severity of neurofibrillary degeneration in the same regions.

Others have suggested that isolating and obtaining volumetric measures of the hippocampus with automated technology is implausible, because of the immense difficulty in delineating this structure (10). We agree that relying on pixel intensity alone is insufficient to correctly identify the hippocampus. Combining knowledge rules of location with pixel intensity, however, results in good delineation of this structure.

One clear advantage of using the automated technology rather than manual tracing is the reduced time and effort required to obtain volumes. Although the manual tracing technique typically required 1 h per brain, the computerized algorithm produces similar estimates in less than 5 min.

We chose to test the validity of KGMAP by using postmortem MR images from participants in the Nun Study, because the availability of detailed quantitative neuropathologic findings permitted us to validate findings against the severity of AD. The strong correlation between quantitative indices of hippocampal AD lesions and the volume of the hippocampus suggests that hippocampal volume determined by KGMAP might be an excellent indicator of the severity of the underlying neuropathologic condition. The 51 cases included in this analysis had a broad distribution of AD neuropathologic conditions and cognitive statuses. Within this group, hippocampal volumes determined by KGMAP strongly correlated with both mean NFT and senile plaque counts in the CA-1 region of the hippocampus and the subiculum, although volumes were best correlated with the severity of neurofibrillary degeneration. Our results concur with those of others who have reported associations of NFT counts with neuronal death and volumetric reduction of the hippocampus (11, 12).

The intraclass correlation for blinded volumetric assessment derived from manual tracing of the right hippocampus was relatively low ($r = 0.64$). Examination of the scatterplot showed that this low correlation was caused by a single outlier. Removal of this outlier from the analyses resulted in an intraclass correlation of 0.88 in the right hippocampus; this finding was similar to the 0.85 correlation obtained in the left hippocampus. When this outlier was removed, the correlation for right hippocampal volume between operator 2 and KGMAP increased to 0.77, which was comparable to the 0.79 correlation for the left hippocampal volume. The fact that all correlations with the outlier removed were similar (≈ 0.80) is encouraging. Further examination revealed that the correlation between the two manual operators was considerably higher when the total volume of the hippocampal and/or amygdala complex was traced ($r = 0.93$). This finding suggested that one of the most important sources of variability in ROI determination of volume is the definition of the boundaries between these structures.

References

1. Convit A, De Leon MJ, Tarshish C, et al. **Specific hippocampal volume reductions in individuals at risk for Alzheimer's disease.** *Neurobiol Aging* 1997;18:131–138
2. Convit A, de Asis J, de Leon MJ, Tarshish CY, De Santi S, Rusinek H. **Atrophy of the medial occipitotemporal, inferior, and middle temporal gyri in non-demented elderly predict decline to Alzheimer's disease.** *Neurobiol Aging* 2000;21:19–26
3. Jack CR Jr, Petersen RC, Xu YC, et al **. Medial temporal atrophy on MRI in normal aging and very mild Alzheimer's disease.** *Neurology* 1997;49:786–794
4. Kaye JA, Swihart T, Howieson D, et al. **Volume loss of the hippocampus and temporal lobe in healthy elderly persons destined to develop dementia.** *Neurology* 1997;48:1297–1304
5. Killiany RJ, Gomez-Isla T, Moss M, et al. **Use of structural magnetic resonance imaging to predict who will get Alzheimer's disease.** *Ann Neurol* 2000;47:430–439
6. Honeycutt NA, Smith CD. **Hippocampal volume measurements using magnetic resonance imaging in normal young adults.** *J Neuroimaging* 1995;5:95–100
7. Snowdon DA, Kemper SJ, Mortimer JA, Greiner LH, Wekstein DR, Markesbery WR. **Linguistic ability in early life and cognitive function and Alzheimer's disease in late life: findings from the Nun Study.** *JAMA* 1996;275:528–532
8. Braak H, Braak E. **Neuropathological stageing of Alzheimer-related changes.** *Acta Neuropathol* 1991;82:239–259
9. Gosche KM, Velthuizen RP, Murtagh FR, et al. **Automated quantification of brain magnetic resonance image hyperintensities using hybrid clustering and knowledge-based methods.** *Int J Imaging Syst Technol* 1999;10:287–293
10. Fox N. **Magnetic resonance imaging in Alzheimer's disease: from diagnosis to measuring therapeutic effect.** *Alzheimer's Reports* 1999;2:5–12
11. Bobinski M, Wegiel J, Wisniewski HM, et al. **Neurofibrillary pathology: correlation with hippocampal formation atrophy in Alzheimer's disease.** *Neurobiol Aging* 1996;17:909–919
12. Bobinski M, de Leon MJ, Tarnawski M, et al. **Neuronal and volume loss in CA1 of the hippocampal formation uniquely predicts duration and severity of Alzheimer's disease.** *Brain Res* 1998;805:267–269